

Infrared Properties of $z=7$ Galaxies from Cosmological Simulations

Renyue Cen¹ and Taysun Kimm²

ABSTRACT

Three-dimensional panchromatic dust radiative transfer calculations are performed on a set of 198 galaxies of stellar masses in the range $5 \times 10^8 - 3 \times 10^{10} M_{\odot}$ from a cosmological hydrodynamic simulation (resolved at $29h^{-1}\text{pc}$) at $z \sim 7$. In a companion paper (Kimm & Cen), the stellar mass and UV luminosity functions, and UV-optical and FUV-NUV colors are shown to be in good agreement with observations, if an SMC-type dust extinction curve is adopted. Here we make useful predictions, self-consistently, of the infrared properties of these $z \sim 7$ simulated galaxies that can be confronted with upcoming ALMA data. Our findings are as follows. (1) The effective radius in the restframe MIPS70 μm band is in the range of 80 – 400pc proper for $z = 7$ galaxies with $L_{\text{FIR}} = 10^{11.3-12} L_{\odot}$. (2) The median of the peak wavelength of the far-infrared (FIR) spectral energy distribution is in the range of 45 – 60 μm , depending on the dust-to-metal ratio. (3) For star formation rate in the range 3 – 100 $M_{\odot} \text{ yr}^{-1}$ the median FIR to bolometric luminosity ratio is 60 – 90%. (4) The FIR luminosity function displays a power law in the high end with a slope of -3.1 ± 0.4 , instead of the usual exponential decline.

Subject headings: Methods: numerical, Galaxies: formation, Galaxies: evolution, Galaxies: interactions, intergalactic medium

1. Introduction

Did stars or quasars reionize the universe? We do not know that for sure, although there is a likelihood that stars most likely dominate the photoionization rate over quasars at $z \geq 6$ (e.g., Faucher-Giguère et al. 2008). While the final transition from an opaque to transparent universe for ionizing photons appears to occur at $z \sim 6$, as seen by the Sloan Digital Sky Survey (SDSS) quasar absorption spectrum observations (e.g., Fan et al. 2006), the reionization process may be quite complex and likely has started much earlier ($z \geq 9$), as suggested by the high Thomson optical depth measured by the Wilkinson Microwave Anisotropy Probe (WMAP) observations (e.g., Hinshaw et al. 2012) and the Planck Surveyor (e.g., Planck Collaboration et al. 2013). To fundamentally answer the question of how the universe was reionized and what reionized it requires a satisfactory understanding of the formation of galaxies during the epoch of reionization.

There have been rapid and remarkable advances on the observational front to address this question, with some of the recent observations penetrating well into the reionization era at $z \sim 6 - 9$

¹Princeton University Observatory, Princeton, NJ 08544; cen@astro.princeton.edu

(e.g., Bouwens et al. 2010; Bunker et al. 2010; Yan et al. 2010; Stark et al. 2010; Labbé et al. 2010; Wilkins et al. 2011; McLure et al. 2011; Dunlop et al. 2012; Bouwens et al. 2012; Finkelstein et al. 2012; Dunlop et al. 2013). They have taught us three important things about the real universe. First, the observed faint end slope of the galaxy luminosity function (LF) is close to -2 , indicating that fainter galaxies below the current detection limit likely make a significant contribution to the overall ionizing photon budget. Second, it appears that star formation in these systems may have started much earlier (Labbé et al. 2010). Third, the stellar mass of detected galaxies is at or above $10^9 M_\odot$, implying halo masses of $\geq 10^{10} M_\odot$ at the current detection limit. The standard cosmological constant-dominated cold dark matter model (Λ CDM) (e.g., Krauss & Turner 1995) predicts that the majority of stars at $z = 6 - 10$ are in small dwarf galaxies residing in halos of mass $\sim 10^8 - 10^{10} M_\odot$ (e.g., Wise & Cen 2009). Thus, it seems likely that the candidate galaxies that are currently detected in the Hubble Ultra Deep Field and Early Release Science (ERS) observations at $z \sim 7 - 8$ may represent the high end of the galaxy mass spectrum.

Can the multi-wavelength predictions of the standard cold dark matter model reproduce the observations? To answer this question, we have performed panchromatic ($\lambda = 0.1 - 1000 \mu\text{m}$) three-dimensional dust radiative transfer calculations on 198 galaxies of stellar mass $5 \times 10^8 - 3 \times 10^{10} M_\odot$ obtained from an ab initio cosmological adaptive mesh refinement hydrodynamic simulation with high resolution ($29 \text{h}^{-1} \text{pc}$). Three parameters are used in the radiative transfer calculation: the dust-to-metal ratio, the extinction curve, and the fraction of directly escaped light from stars (f_{esc}). In Kimm & Cen (2013) we show that our stellar mass function is in broad agreement with González et al. (2011), independent of the three parameters. We also show that our simulated galaxies can reasonably and simultaneously match the observed UV-optical color, UV spectral slope and the UV luminosity function, if $f_{\text{esc}} \sim 10\%$ and a Small Magellanic Cloud (SMC)-type extinction curve is used. The conclusion that the model with $f_{\text{esc}} \sim 10\%$ is favored over the model with much smaller f_{esc} is encouraging based on independent considerations. Observations of cosmological reionization infer the Thomson optical depth $\tau_e = 0.089 \pm 0.014$ (Hinshaw et al. 2012), indicating a reionization redshift of $z_{re} = 10.6 + 1.1$ (assuming a sudden reionization picture). In order to reionize the universe at this redshift range by stellar sources, $f_{\text{esc}} \ll 10\%$ would not be viable (e.g., Cen 2003). Moreover, detailed radiative transfer simulations with still higher resolutions indicate a porous interstellar medium, and $f_{\text{esc}} \sim 10\%$ is within the range of predictions for galaxies at high redshift (e.g., Wise & Cen 2009; Razoumov & Sommer-Larsen 2010; Yajima et al. 2011).

One interesting and perhaps not entirely expected property, according to the conventional wisdom, that comes from our calculations is that most of these simulated galaxies are heavily dust-attenuated with extinction of $1 \leq A_{\text{FUV}} \leq 5$. This indicates that a significant amount of stellar radiation may be re-processed by dust and seen in the FIR. The questions are then: Does the star formation rate (SFR) inferred based on the observed optical and UV luminosities nearly account for the total SFR? What are their infrared properties that can be checked by upcoming ALMA observations (e.g., Carilli et al. 2008; Hodge et al. 2013)? This paper addresses these two questions. The outline of this paper is as follows. In §2 we detail our simulations (§2.1), method of making galaxy catalogs (§2.2) and panchromatic three-dimensional dust radiative transfer method (§2.3). Results are presented in §3. Conclusions are given in §4.

2. Simulations

2.1. Hydrocode and Simulation Parameters

The cosmological simulation is performed with the Eulerian hydrodynamics code, ENZO (Bryan 1999; O’Shea et al. 2005; Joung et al. 2009). For more details on the simulation setup and implemented physics, the reader is referred to Cen (2012). We use the following cosmological parameters that are consistent with the WMAP7-normalized (Komatsu et al. 2010) Λ CDM model: $\Omega_M = 0.28$, $\Omega_b = 0.046$, $\Omega_\Lambda = 0.72$, $\sigma_8 = 0.82$, $H_0 = 100h \text{ km s}^{-1}\text{Mpc}^{-1} = 70 \text{ km s}^{-1}\text{Mpc}^{-1}$ and $n = 0.96$. These parameters are consistent with those from Planck first-year data (Planck Collaboration et al. 2013) if we average Planck derived H_0 with SN Ia and HST based H_0 . First we ran a low resolution simulation with a periodic box of $120 h^{-1}\text{Mpc}$ (comoving) on a side. We identified a region centered on a cluster of mass of $\sim 3 \times 10^{14} M_\odot$ at $z = 0$. We then resimulate with high resolution of the chosen region embedded in the outer $120h^{-1}\text{Mpc}$ box to properly take into account the large-scale tidal field and appropriate boundary conditions at the surface of the refined region. The refined region has a comoving size of $21 \times 24 \times 20h^{-3}\text{Mpc}^3$ and represents 1.8σ matter density fluctuation on that volume. The dark matter particle mass in the refined region is $1.3 \times 10^7 h^{-1} M_\odot$. The refined region is surrounded by three layers (each of $\sim 1h^{-1}\text{Mpc}$) of buffer zones with particle masses successively larger by a factor of 8 for each layer, which then connects with the outer root grid that has a dark matter particle mass 8^4 times that in the refined region. We choose the mesh refinement criterion such that the resolution is always better than $29h^{-1}\text{pc}$ (physical), corresponding to a maximum mesh refinement level of 13 at $z = 0$. The simulations include a metagalactic UV background (Haardt & Madau 1996) where the cosmic reionization occurs at $z = 9$, and a model for shielding of UV radiation (Cen et al. 2005). They include metallicity-dependent radiative cooling (Cen et al. 1995). Our simulations also solve relevant gas chemistry chains for molecular hydrogen formation (Abel et al. 1997), molecular formation on dust grains (Joung et al. 2009), and metal cooling extended down to 10 K (Dalgarno & McCray 1972). Star particles are created in cells that satisfy a set of criteria for star formation proposed by Cen & Ostriker (1992). Each star particle is tagged with its initial mass, creation time, and metallicity; star particles typically have masses of $\sim 10^6 M_\odot$.

Supernova feedback from star formation is modeled following Cen et al. (2005). Feedback energy and ejected metal-enriched mass are distributed into 27 local gas cells centered at the star particle in question, weighted by the specific volume of each cell. This is to mimic the physical process of supernova blastwave propagation that tends to channel energy, momentum and mass into the least dense regions (with the least resistance and cooling). The primary advantages of this supernova energy based feedback mechanism are three-fold. First, nature does drive winds in this way and energy input is realistic. Second, it has only one free parameter e_{SN} , namely, the fraction of the rest mass energy of stars formed that is deposited as thermal energy on the cell scale at the location of supernovae. Third, the processes are treated physically, obeying their respective conservation laws (where they apply), allowing transport of metals, mass, energy and momentum to be treated self-consistently and taking into account relevant heating/cooling processes at all times. We allow the entire feedback processes to be hydrodynamically coupled to surroundings and subject to relevant physical processes, such as cooling and heating. The total amount of explosion

kinetic energy from Type II supernovae for an amount of star formed M_* with a Chabrier initial mass function (IMF) is $e_{SN}M_*c^2$ (where c is the speed of light) with $e_{SN} = 6.6 \times 10^{-6}$. Taking into account the contribution of prompt Type I supernovae, we use $e_{SN} = 1 \times 10^{-5}$ in our simulations. Observations of local starburst galaxies indicate that nearly all of the star formation produced kinetic energy is used to power galactic superwinds (e.g., Heckman 2001). Supernova feedback is important primarily for regulating star formation and for transporting energy and metals into the intergalactic medium. The extremely inhomogeneous metal enrichment process demands that both metals and energy (and momentum) are correctly modeled so that they are transported in a physically sound (albeit still approximate at the current resolution) way.

2.2. Simulated Galaxy Catalogs

We identify galaxies in our high resolution simulations using the HOP algorithm (Eisenstein & Hu 1999), operated on the stellar particles, which is tested to be robust and insensitive to specific choices of concerned parameters within reasonable ranges. Satellites within a galaxy are clearly identified separately. The luminosity of each stellar particle at each of the Sloan Digital Sky Survey (SDSS) five bands is computed using the GISSEL stellar synthesis code (Bruzual & Charlot 2003), by supplying the formation time, metallicity and stellar mass. Collecting luminosity and other quantities of member stellar particles, gas cells and dark matter particles yields the following physical parameters for each galaxy: position, velocity, total mass, stellar mass, gas mass, mean formation time, mean stellar metallicity, mean gas metallicity, star formation rate, luminosities in five SDSS bands (and various colors) and others.

2.3. Three-Dimensional Panchromatic Dust Radiative Transfer Calculations

We post-process the simulated galaxy sample at $z = 7$ using a three-dimensional dust radiation transfer code, SUNRISE (Jonsson 2006; Jonsson et al. 2010). The main strength of the SUNRISE code is the use of a polychromatic algorithm to trace information in all wavelengths per ray, enabling us to compute the spectral energy distributions (SEDs) of each galaxy. It makes use of the standard dust cross-sections by Draine and collaborators (Weingartner & Draine 2001; Draine & Li 2007) to simulate absorption and multiple scattering by dust. Each stellar particle that is basically a coeval star cluster has three attributes - mass ($\sim 10^{4-5} M_\odot$), formation time and metallicity - which are input to the code STARBURST99 (Leitherer et al. 1999), assuming a Kroupa initial mass function with an upper (lower) mass limit of $100 M_\odot$ ($0.1 M_\odot$). The output from STARBURST99 is the input stellar spectrum to SUNRISE. In order to take into account the immediate absorption and emission by birth clouds, which large-scale cosmological simulations cannot resolve, SUNRISE uses the spectra of HII and photo-dissociation regions (PDRs) computed by photo-ionization code, MAPPINGSIII (Dopita et al. 2005; Groves et al. 2008). This is done by replacing SEDs of star particles younger than 10 Myr with re-processed SEDs of a population with constant star formation for 10 Myr by MAPPINGSIII (see Jonsson et al. 2010). The fraction of light travelled through the PDR is controlled by a parameter, f_{PDR} , which we use $f_{\text{PDR}} = 0.2$ following Jonsson et al. (2010).

The metal mass in each simulation cell is followed hydrodynamically, including flux, sources (from stellar feedback) and sinks (forming into new stars). The amount of dust is derived from the amount of metals in each hydro cell by using a dust-to-metal ratio (D/M). While the UV/optical properties depend sensitively on D/M , the FIR properties depends on D/M only weakly, as will be shown, making our predictions of FIR properties of $z = 7$ rather robust, except the peak wavelength of the FIR SED (see Figure 2 below). The dust temperature, emission, and dust opacity is obtained in a self-consistent fashion in SUNRISE by solving for the thermal equilibrium solution for dust grains at every location, where dust emission cooling is balanced by stellar radiative heating. This is achieved by iteration computationally.

3. Results

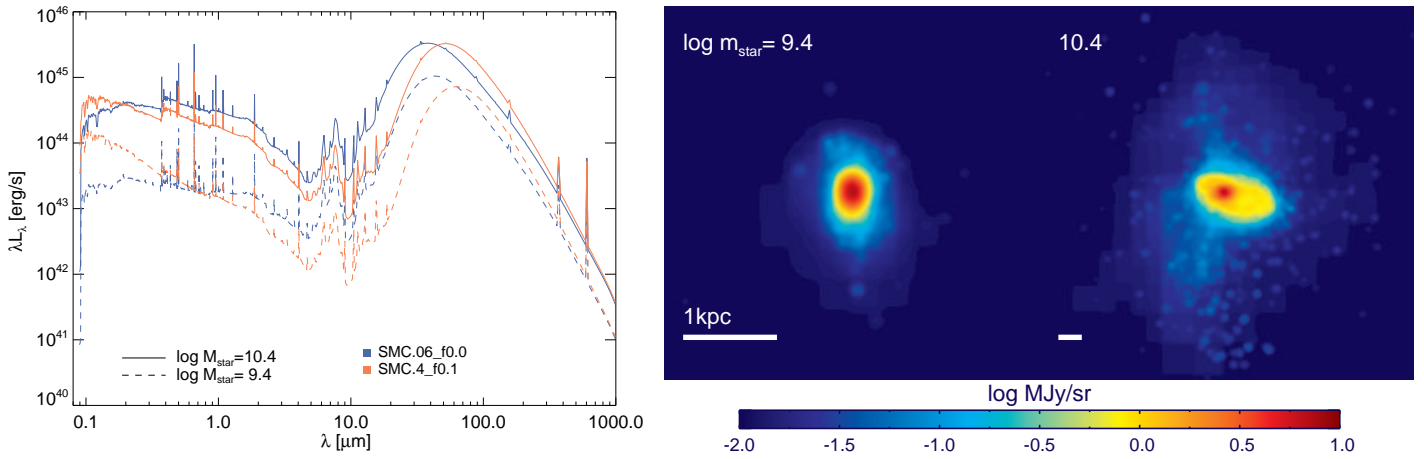


Fig. 1.— Left panel: the rest-frame spectra (left panel) of two simulated galaxies of stellar masses of $10^{9.4} M_{\odot}$ (dashed curves) and $10^{10.4} M_{\odot}$ (solid curves), respectively, at $z = 7$. The star formation rate (SFR) and specific SFR (sSFR) for the low and high mass galaxies are ($94 M_{\odot}/\text{yr}$, 3.7 Gyr^{-1}) and ($35 M_{\odot}/\text{yr}$, 13 Gyr^{-1}), respectively. For each galaxy we show two cases with two different combinations of $(D/M, f_{\text{esc}})$, $(0.4, 0.1)$ (red) and $(0.06, 0)$ (blue), both of which are found to reproduce the UV/optical properties of $z = 7$ galaxies (Kimm & Cen 2013). Right panel: restframe MIPS $70\mu\text{m}$ band images, smoothed with a Gaussian of $\text{FWHM}=0.1\text{kpc}$. The number in each panel indicates logarithmic stellar mass and white ticks in both panels are 1kpc proper.

We first present in Figure 1 the SED in the rest-frame and rest-frame FIR images of two simulated galaxies of stellar masses of $10^{9.4} M_{\odot}$ and $10^{10.4} M_{\odot}$, respectively. For each galaxy we show two cases with two different combinations of $(D/M, f_{\text{esc}})$, $(0.4, 0.1)$ (red) and $(0.06, 0)$ (blue), which have been both found to reproduce the UV/optical properties of $z = 7$ galaxies (Kimm & Cen 2013). Three points are worth noting. First, the overall SED shares some of the properties of lower redshift starburst galaxies, in that the majority of the stellar radiation comes out in the FIR peak. Second, even though the two galaxies are in the category of starburst galaxies, the higher mass galaxy contains a significant, evolved stellar population, as indicated by a strong Balmer break at $\sim 0.37\mu\text{m}$; the lower mass galaxy has a less prominent Balmer break, suggesting an overall

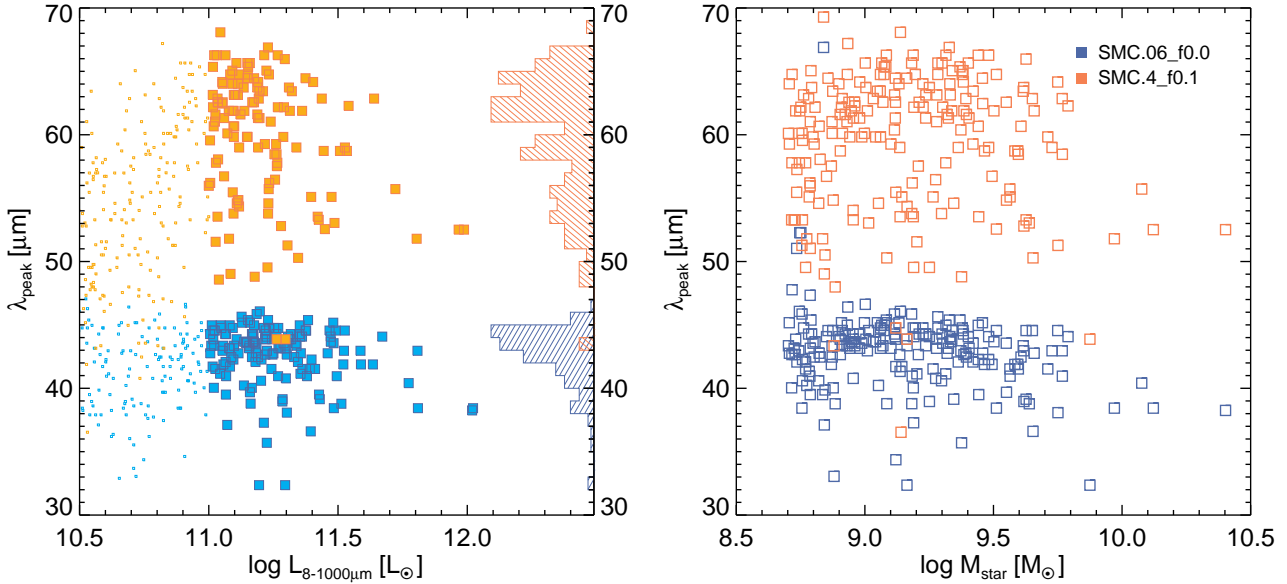


Fig. 2.— shows the FIR peak wavelength λ_{peak} of the SED of galaxies at $z = 7$ as a function of FIR luminosity (left panel) and stellar mass (right panel). Only galaxies with stellar masses $M_{\text{star}} \geq 5 \times 10^8 M_{\odot}$ are shown. For each galaxy two cases are shown with two different combinations of $(D/M, f_{\text{esc}})$, $(0.4, 0.1)$ (red) and $(0.06, 0)$ (blue). The distributions of λ_{peak} are shown on the right y-axis for the two cases. The histogram in the left panel is plotted using the sample with $L_{8-1000\mu\text{m}} \geq 10^{11} L_{\odot}$ over which our sample is more than 80% complete. The completeness is estimated as follows. At IR luminosity of $\geq 10^{11} L_{\odot}$ we compute the fraction of galaxies with stellar masses larger than $5 \times 10^8 M_{\odot}$ (which is our stellar mass threshold deemed reliably resolved), which is found to be 80%.

younger population. The existence of an evolved population for $z \sim 7$ galaxies is consistent with observations (e.g., Labbé et al. 2010). It is likely that our simulation has underestimated the star formation rate at progressively higher redshift due to poorer resolutions for smaller objects at higher redshift, hence the evolved population. Third, the wavelength λ_{peak} of the FIR peak at $45 - 65 \mu\text{m}$ suggests a relatively hot emitting dust, due to a combination of relatively high SFR and sub-kpc, compact sizes of the starbursting regions, seen in the images in the right panel.

Figure 2 shows the FIR peak wavelength λ_{peak} of the SED of the galaxies at $z = 7$ as a function of FIR luminosity (left panel) and stellar mass (right panel). For each galaxy two cases are shown with two different combinations of $(D/M, f_{\text{esc}})$, $(0.4, 0.1)$ (red) and $(0.06, 0)$ (blue). The distributions of λ_{peak} are shown on the right y-axis for the two cases. Two points are noted. First, at the lower stellar mass ($\leq 10^{10} M_{\odot}$) or lower FIR luminosity end ($L_{\text{FIR}} \leq 10^{11.5} L_{\odot}$), no strong correlation is found between either FIR luminosity or stellar mass and λ_{peak} , whereas there is some hint that the highest FIR luminosity ($L_{\text{FIR}} \geq 10^{11.5} L_{\odot}$) or highest stellar mass ($\geq 10^{10} M_{\odot}$) galaxies tend to occupy the low end of the λ_{peak} distribution. Second, for a given simulated galaxy, post-processing it with different dust-to-metal ratios D/M yields significant difference in the λ_{peak} distributions. For the lower $D/M = 0.06$ case, the median of the λ_{peak} distribution is $43 \mu\text{m}$, compared to $61 \mu\text{m}$ for the case with $D/M = 0.4$. This significant dependence of λ_{peak} on D/M may provide a probe

of the latter, when the former is observationally obtained. The physical origin for this, in simple terms, is that a lower D/M value gives a lower dust opacity hence a higher interstellar radiation field, which in turn heats up the dust to a higher equilibrium temperature (balanced by emission cooling, primarily).

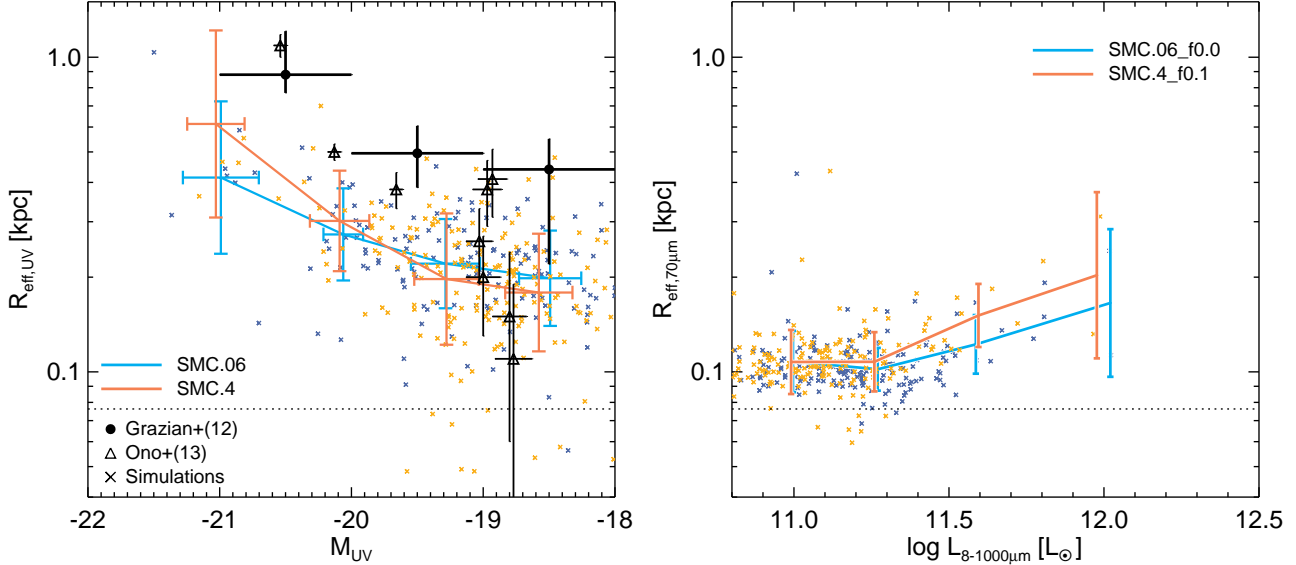


Fig. 3.— Left: FUV effective radius measured after smoothing with a Gaussian of FWHM=0.1 kpc as a function of GALEX FUV magnitude for simulated galaxies at $z = 7$. Included as black symbols are observational estimates by Grazian et al. (2012, circles) and Ono et al. (2012, triangles). Right: effective radius in FIR as a function of FIR luminosity for galaxies at $z = 7$. The effective radius is measured on restframe MIPS 70 μm band images after smoothing with a Gaussian of FWHM=0.1 kpc. The dotted line marks the effective resolution of our simulation (75 pc). The solid lines and error bars indicate the mean and standard deviation.

We examine the sizes of simulated $z = 7$ galaxies. We first examine UV sizes. The left panel of Figure 3 shows the effective radius in GALEX FUV band as a function of FUV magnitude. We see that the simulated galaxies have somewhat smaller sizes than the observed counterparts in the rest-frame FUV band, although the trend that more UV luminous galaxies have larger sizes is in agreement with observations and there is significant overlap between observations and our simulation. The red curve with $f_{\text{esc}} = 10\%$ is actually computed not including the 10% directly escaped light, because we are unsure how to best model it without introducing some additional unchecked parameters. We now turn to FIR sizes of simulated $z = 7$ galaxies, shown in the right panel of Figure 3. What is striking is that the predicted sizes of $z = 7$ galaxies in the FIR band are very small, with effective radii being in the range of 80 – 500pc proper. The effective resolution of our simulation is 75pc [1.8 cells, see Cen (2013)], which is probably the cause of the size floor seen. Thus, we expect the lower mass galaxies may have effective radii in FIR that are smaller than $\sim 80\text{pc}$. Nevertheless, we expect that the sizes in the range 100 – 500pc predicted to be real, to the extent that our simulation resolution is adequate for resolving them. Because the FIR emission is primarily a function of the metal density distribution in the simulated galaxies, they are much less prone to attenuation effects and hence are more robust. However, there are possible

caveats that the reader should keep in mind. The central star formation may be dependent on feedback processes from star formation. Since the exact strength of stellar feedback depends on an array of factors that each have significant uncertainties, including the initial stellar mass function (IMF), supernova feedback prescription used in the simulation, porosity of the interstellar medium in the simulation that may be underestimated, feedback from AGN that is not included, etc, our best estimate is that the sizes of the simulated galaxies may have been underestimated somewhat presently. A comparison between our simulated results and upcoming observations will thus shed useful light on both the cosmological model and astrophysics of galaxy formation at high redshift.

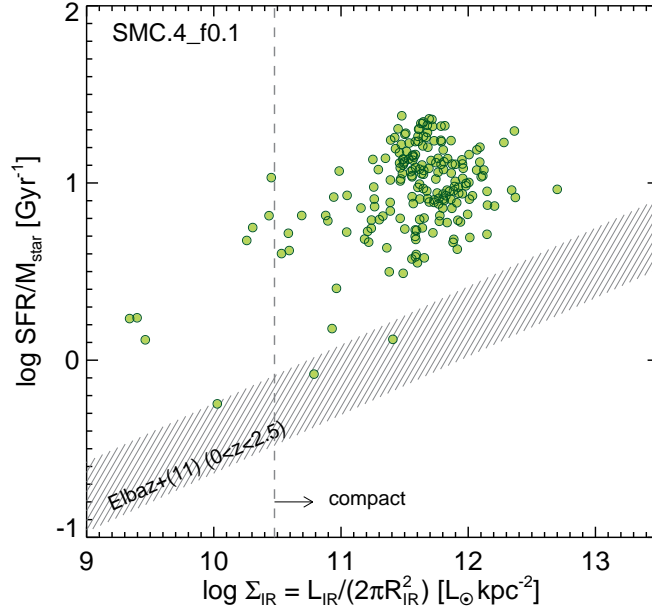


Fig. 4.— shows the sSFR as a function of FIR surface brightness (Σ_{IR}) for simulated galaxies at $z = 7$ (circles). Σ_{IR} is computed as $L_{8-1000\mu\text{m}}/2\pi R_{\text{IR}}^2$, where R_{IR} is the effective radius in the restframe MIPS $70\ \mu\text{m}$ band. Only one dust model is shown, because Σ_{IR} is insensitive to details of the dust model. For comparisons, also shown as the shaded region is the star-forming sequence from the GOODS-Herschel sample at $0 < z < 2.5$ (Elbaz et al. 2011).

Another way to demonstrate the concentration of star formation in $z = 7$ galaxies is to plot the specific star formation rate as a function of FIR surface brightness, shown in Figure 4. Comparing to the galaxies in the star-forming sequence at moderate redshift ($0 < z < 2.5$) (Elbaz et al. 2011), it is evident that our simulated galaxies at $z = 7$ are substantially more star-bursting by a factor of 3 – 20 at a fixed surface density. Elbaz et al. (2011) also defines a galaxy as “compact” if the FIR surface brightness ($\Sigma_{\text{IR}} = L_{\text{IR}}/2\pi R_{\text{IR}}^2$) is greater than $3 \times 10^{10} L_{\odot} \text{ kpc}^{-2}$. This roughly corresponds to galaxies emitting more than 60% of their $13.2\ \mu\text{m}$ flux in the unresolved central $\sim 3\ \text{kpc}^2$ region (see Díaz-Santos et al. 2010). According to the definition, the majority of the simulated galaxies will be classified as compact galaxies.

Having examined the SEDs and sizes, our attention is shifted to the FIR radiation output of $z = 7$ galaxies relative to their bolometric luminosities. Figure 5 shows FIR in the range $8-1000\ \mu\text{m}$ (left panel) and bolometric (right panel) luminosities of each galaxy at $z = 7$ as a function of the

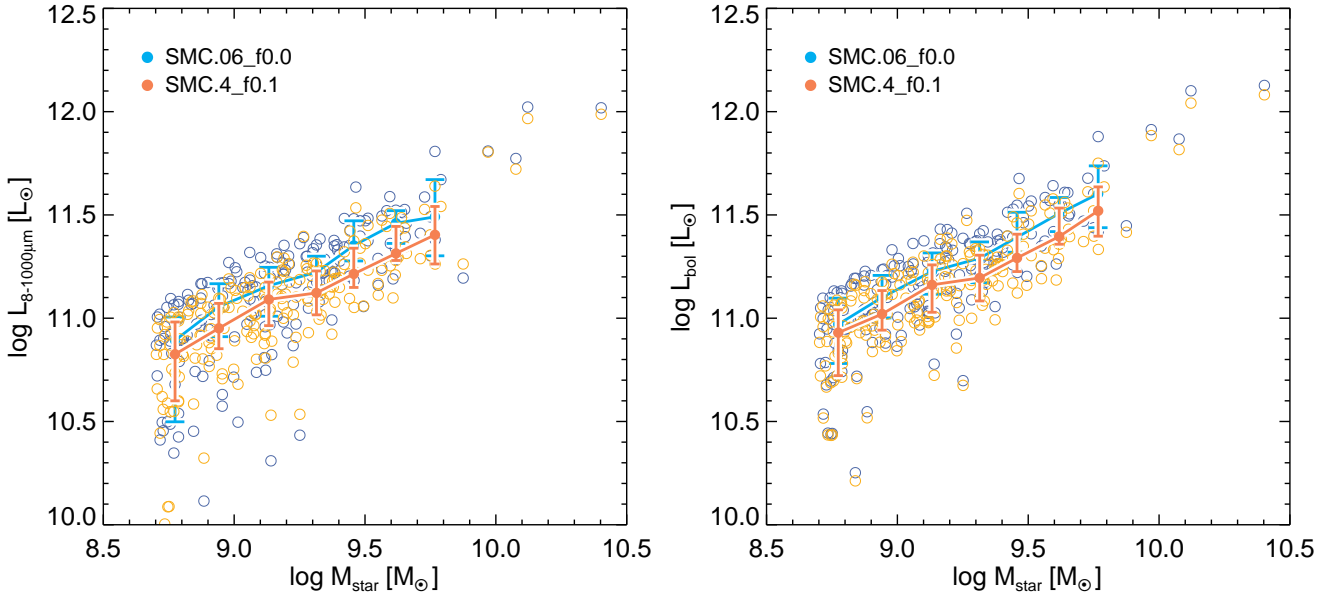


Fig. 5.— shows FIR (left) and bolometric (right) luminosities in the range 8–1000 μm of each galaxy at $z = 7$ as a function of the galaxy stellar mass, for two models with $(D/M, f_{\text{esc}})$, (0.4,0.1) (red open circles) and (0.06,0) (blue open circles). Solid points with error bars represent the median and interquartile range.

galaxy stellar mass, for two models with $(D/M, f_{\text{esc}})$, (0.4,0.1) (red open circles) and (0.06,0) (blue open circles). Let us first study the right panel. It is evident that bolometric luminosity (i.e., SFR) scales with stellar mass substantially sublinearly, $L_{\text{bol}} \propto M_{\text{star}}^{\xi}$ with $\xi \sim 0.6 - 0.8$. We attribute this, primarily, to “stochasticity” of star formation, where galaxies with higher specific star formation are in some “bursting periods”, while those with relatively lower specific star formation rates presently are in relatively quiet “patches”. This explanation is consistent with the ~ 0.5 dex spread in the bolometric luminosity at a fixed stellar mass. The relation between FIR luminosity and stellar mass (left panel) is largely inherited from that of between bolometric luminosity and stellar mass (right panel), with a small correction due to a non-uniform ratio of FIR to bolometric luminosities, shown in Figure 6 below. If confirmed by ALMA, this will provide significant insight into the galaxy formation process at high redshift. The expectation is that, with time, galaxies will mature and become stellar mass dominated on the baryon budget, and as such, the overall stochasticity is expected to decline towards lower redshift, resulting in ξ gradually approaching unity.

Figure 6 shows the ratio of FIR luminosity in the range 8–1000 μm to the bolometric luminosity for each galaxy as a function of stellar mass (left) and star formation rate (right), for two models with a dust-to-metal ratio (D/M) of 0.06 and 0.4. It is seen that there is a tendency for less massive galaxies or lower SFR galaxies to have lower median ratios. For galaxies with $\text{SFR} = 3 - 100 M_{\odot}/\text{yr}$, it is found that the median FIR/bolometric luminosity ratio is in the range of 60–90%. For galaxies with stellar mass in the range of $10^9 - 10^{10.5} M_{\odot}$, the median FIR/bolometric luminosity ratio is predicted to be in the range of 80–90%. We expect that targeted observations of current high redshift galaxies at $z \sim 7$ by ALMA should be able to verify these predictions.

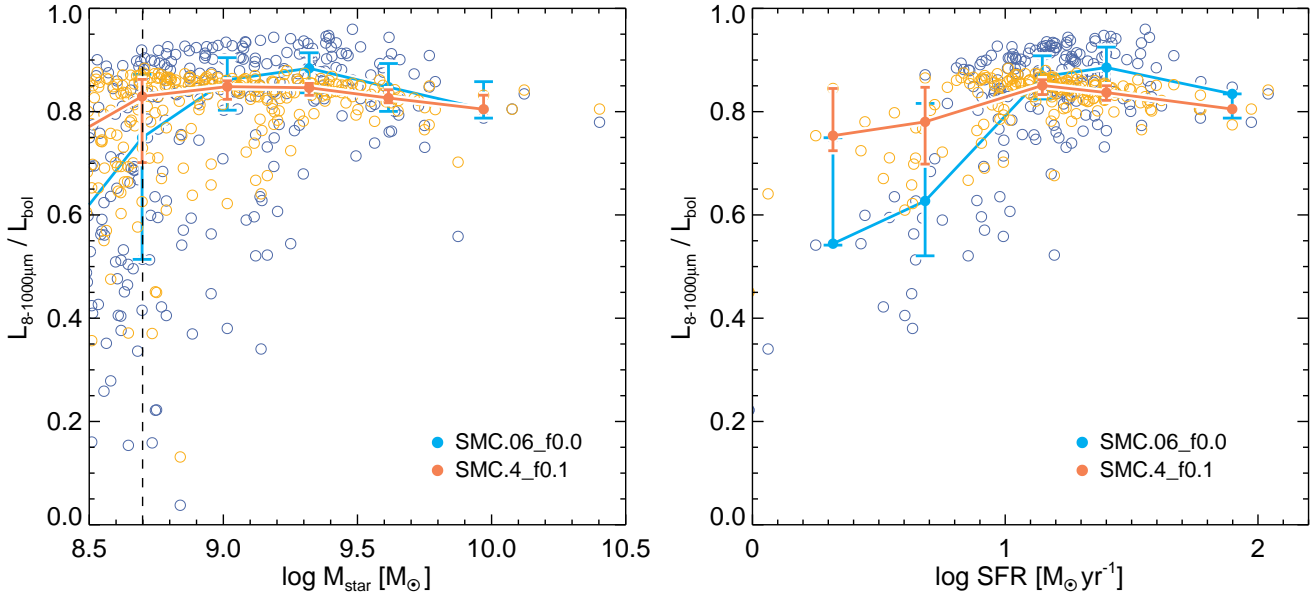


Fig. 6.— The ratio of FIR luminosity appearing in the range $8 - 1000\mu\text{m}$ to the bolometric luminosity as a function of stellar mass (left) and star formation rate (right). Blue and red circles denote the model with a dust-to-metal ratio (D/M) of 0.06 and 0.4, respectively, as indicated in the legend. An SMC-type dust extinction curve is used in both cases. Points with error bars represent median and interquartile range.

Figure 7 shows the galaxy FIR luminosity function at $z = 7$. It is seen that the FIR luminosity function only depends weakly on the changes of dust properties; the two dust models that are found to be able to match UV/optical properties of galaxies at $z = 7$ are shown to give similar results. Interestingly, for the high end luminosity range probed, $L_{\text{FIR}} = 10^{11} - 10^{12} L_{\odot}$, there is no indication of an exponential drop that is normally the case for galaxy stellar mass function or UV/optical luminosity function at high redshift. We find that a power-law slope of -2.1 ± 0.4 provides a good fit to our simulated FIR luminosity functions, where the uncertainty is measured by bootstrap resampling. This power-law shape is related to the stochasticity of star formation of $z = 7$ galaxies, as noted above, which will have significant implications on small-scale power in the standard cold dark matter model as well as the consumption and thermodynamic state of the gas prior to star formation in galaxies at $z = 7$. It is expected that observing the UV selected high redshift galaxy candidates in the UDF by ALMA may be able to check this expected power-law slope. It is noted that, since the ratio of FIR to bolometric luminosity is close to unity (see Figure 6), this power-law behavior is rather robust to attenuation uncertainties that plague rest-frame UV luminosity functions, making FIR continuum observations by ALMA especially powerful. If verified, we will learn a great deal of the mode of star formation in high- z galaxies: how bursty is star formation in high redshift galaxies and what is the dispersion in star formation rate at a fixed halo or stellar mass?

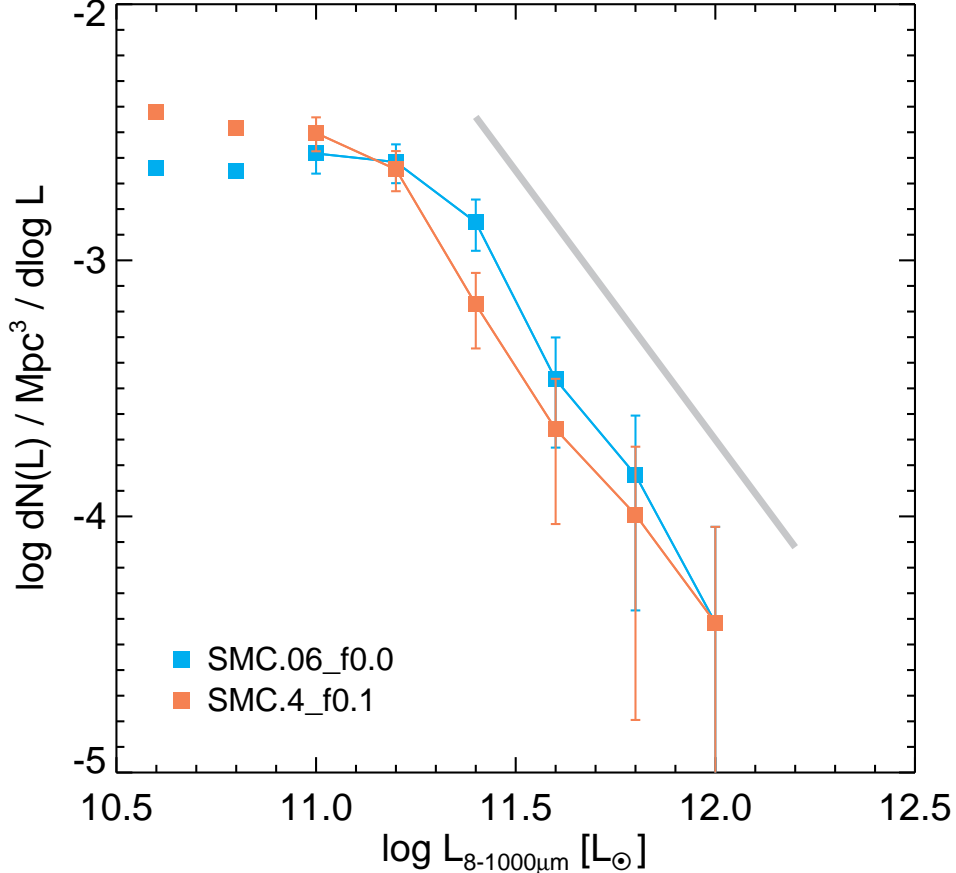


Fig. 7.— The infrared luminosity function at $z = 7$. Different color-codings correspond to models with a different assumption on D/M , as indicated in the legend. Solid lines display our reliable estimates for the number density, which can be directly compared to future observations. Other two bins below $L_{8-1000\mu m} = 10^{11}L_{\odot}$ contain more than 20% of under-resolved galaxies of stellar mass $M_{\text{star}} < 2 \times 10^8 M_{\odot}$. 1σ error bars shown are Poissonian. The simulated LFs can be fit by a power law [$\log dN \propto (-2.1 \pm 0.4)d\log L$], shown as the gray line.

4. Conclusions

We perform, in unprecedented details, three-dimensional panchromatic dust radiative transfer calculations on a set of 198 galaxies of stellar masses in the range $5 \times 10^8 - 3 \times 10^{10} M_{\odot}$ resolved at $29h^{-1}\text{pc}$ at $z \sim 7$ from an *ab initio* cosmological hydrodynamic simulation of the standard cold dark matter model. The soundness of treatment of relevant physical processes has been checked by comparing to a set of independent observations. In a companion paper (Kimm & Cen 2013) we show that the UV-optical properties, including stellar mass and luminosity functions, UV-optical and FUV-NUV colors, are in good agreement with observations, if an SMC-type dust extinction curve is adopted. In order to make further testable predictions of the same model, we present here, self-consistently, an additional set of infrared continuum properties of these $z \sim 7$ simulated galaxies, to be confronted with upcoming ALMA data. The main results may be summarized in

four points.

(1) The effective radius in the restframe MIPS70 μ m band is in the range of 80 – 400pc proper for $z = 7$ galaxies with $L_{\text{FIR}} = 10^{11.3-12} L_{\odot}$, corresponding to an angular size of $0''.015 - 0''.075$, which may be resolvable by ALMA. The majority of the simulated galaxies would be classified as compact starburst galaxies (Elbaz et al. 2011). The predicted size would be below the extrapolation from lower redshift evolution in rest-frame UV or visual band (e.g., Ferguson et al. 2004; Trujillo et al. 2006).

(2) The median of the peak wavelength of the FIR SED is in the range of 45 – 60 μ m, depending on the dust-to-metal ratio, corresponding to observed wavelength of 360 – 480 μ m, within the ALMA range. The peak wavelength found is comparable to local starburst galaxies, such as Arp 220 and NGC 6240.

(3) For galaxies with SFR in the range 3 – 100 $M_{\odot} \text{ yr}^{-1}$, the median FIR in the range 8–1000 μ m to bolometric luminosity ratio is 60 – 90%. In other words, the SFR inferred based on the observed optical and UV luminosities is missing more than one half of the total SFR, on average. This is a new and key prediction that should be easily verifiable by upcoming ALMA observations, in conjunction with HST UDF data.

(4) The FIR luminosity function displays a power law in the high end with a slope of -3.1 ± 0.4 , instead of the usual exponential decline. A related result is that $L_{\text{bol}} \propto M_{\text{star}}^{\xi}$ with $\xi \sim 0.6 - 0.8$, which is somewhat flatter than the corresponding relation at lower redshifts. Both results may be attributable to “stochasticity” and significant dispersions in star formation at a given halo mass.

Acknowledgements

We would like to thank Bruce Draine, Simona Gallerani, Roberto Maiolino and John Wise for discussion, and an anonymous referee for a very useful constructive report. Computing resources were in part provided by the NASA High- End Computing (HEC) Program through the NASA Advanced Supercomputing (NAS) Division at Ames Research Center. The research is supported in part by NSF grant AST-1108700 and NASA grant NNX12AF91G. Some of our analysis is done using the YT toolkit (Turk et al. 2011).

REFERENCES

- Abel, T., Anninos, P., Zhang, Y., & Norman, M. L. 1997, *New Astronomy*, 2, 181
- Bouwens, R. J., Illingworth, G. D., Oesch, P. A., Franx, M., Labbé, I., Trenti, M., van Dokkum, P., Carollo, C. M., González, V., Smit, R., & Magee, D. 2012, *ApJ*, 754, 83
- Bouwens, R. J., Illingworth, G. D., Oesch, P. A., Labbe, I., Trenti, M., van Dokkum, P., Franx, M., Stiavelli, M., Carollo, C. M., Magee, D., & Gonzalez, V. 2010, *ArXiv e-prints*
- Bruzual, G., & Charlot, S. 2003, *MNRAS*, 344, 1000

- Bryan, G. L. 1999, *Comput. Sci. Eng.*, Vol. 1, No. 2, p. 46 - 53, 1, 46
- Bunker, A. J., Wilkins, S., Ellis, R. S., Stark, D. P., Lorenzoni, S., Chiu, K., Lacy, M., Jarvis, M. J., & Hickey, S. 2010, *MNRAS*, 1378
- Carilli, C. L., Walter, F., Wang, R., Wootten, A., Menten, K., Bertoldi, F., Schinnerer, E., Cox, P., Beelen, A., & Omont, A. 2008, *Ap&SS*, 313, 307
- Cen, R. 2003, *ApJ*, 591, 12
- . 2012, *ApJ*, 748, 121
- . 2013, ArXiv e-prints
- Cen, R., Kang, H., Ostriker, J. P., & Ryu, D. 1995, *ApJ*, 451, 436
- Cen, R., Nagamine, K., & Ostriker, J. P. 2005, *ApJ*, 635, 86
- Cen, R., & Ostriker, J. P. 1992, *ApJ*, 399, L113
- Dalgarno, A., & McCray, R. A. 1972, *ARA&A*, 10, 375
- Díaz-Santos, T., Charmandaris, V., Armus, L., Petric, A. O., Howell, J. H., Murphy, E. J., Mazzarella, J. M., Veilleux, S., Bothun, G., Inami, H., Appleton, P. N., Evans, A. S., Haan, S., Marshall, J. A., Sanders, D. B., Stierwalt, S., & Surace, J. A. 2010, *ApJ*, 723, 993
- Dopita, M. A., Groves, B. A., Fischera, J., Sutherland, R. S., Tuffs, R. J., Popescu, C. C., Kewley, L. J., Reuland, M., & Leitherer, C. 2005, *ApJ*, 619, 755
- Draine, B. T., & Li, A. 2007, *ApJ*, 657, 810
- Dunlop, J. S., McLure, R. J., Robertson, B. E., Ellis, R. S., Stark, D. P., Cirasuolo, M., & de Ravel, L. 2012, *MNRAS*, 420, 901
- Dunlop, J. S., Rogers, A. B., McLure, R. J., Ellis, R. S., Robertson, B. E., Koekemoer, A., Dayal, P., Curtis-Lake, E., Wild, V., Charlot, S., Bowler, R. A. A., Schenker, M. A., Ouchi, M., Ono, Y., Cirasuolo, M., Furlanetto, S. R., Stark, D. P., Targett, T. A., & Schneider, E. 2013, *MNRAS*, 432, 3520
- Eisenstein, D., & Hu, P. 1999, *ApJ*, 511, 5
- Elbaz, D., Dickinson, M., Hwang, H. S., Díaz-Santos, T., Magdis, G., Magnelli, B., Le Borgne, D., Galliano, F., Pannella, M., Chianal, P., Armus, L., Charmandaris, V., Daddi, E., Aussel, H., Popesso, P., Kartaltepe, J., Altieri, B., Valtchanov, I., Coia, D., Dannerbauer, H., Dasyra, K., Leiton, R., Mazzarella, J., Alexander, D. M., Buat, V., Burgarella, D., Chary, R.-R., Gilli, R., Ivison, R. J., Juneau, S., Le Floc’h, E., Lutz, D., Morrison, G. E., Mullaney, J. R., Murphy, E., Pope, A., Scott, D., Brodwin, M., Calzetti, D., Cesarsky, C., Charlot, S., Dole, H., Eisenhardt, P., Ferguson, H. C., Förster Schreiber, N., Frayer, D., Giavalisco, M., Huynh, M., Koekemoer, A. M., Papovich, C., Reddy, N., Surace, C., Teplitz, H., Yun, M. S., & Wilson, G. 2011, *A&A*, 533, A119

- Fan, X., Strauss, M. A., Becker, R. H., White, R. L., Gunn, J. E., Knapp, G. R., Richards, G. T., Schneider, D. P., Brinkmann, J., & Fukugita, M. 2006, *AJ*, 132, 117
- Faucher-Giguère, C., Lidz, A., Hernquist, L., & Zaldarriaga, M. 2008, *ApJ*, 688, 85
- Ferguson, H. C., Dickinson, M., Giavalisco, M., Kretchmer, C., Ravindranath, S., Idzi, R., Taylor, E., Conselice, C. J., et al. 2004, *ApJ*, 600, L107
- Finkelstein, S. L., Papovich, C., Salmon, B., Finlator, K., Dickinson, M., Ferguson, H. C., Giavalisco, M., Koekemoer, A. M., Reddy, N. A., Bassett, R., Conselice, C. J., Dunlop, J. S., Faber, S. M., Grogin, N. A., Hathi, N. P., Kocevski, D. D., Lai, K., Lee, K.-S., McLure, R. J., Mobasher, B., & Newman, J. A. 2012, *ApJ*, 756, 164
- González, V., Labbé, I., Bouwens, R. J., Illingworth, G., Franx, M., & Kriek, M. 2011, *ApJ*, 735, L34
- Grazian, A., Castellano, M., Fontana, A., Pentericci, L., Dunlop, J. S., McLure, R. J., Koekemoer, A. M., Dickinson, M. E., Faber, S. M., Ferguson, H. C., Galametz, A., Giavalisco, M., Grogin, N. A., Hathi, N. P., Kocevski, D. D., Lai, K., Newman, J. A., & Vanzella, E. 2012, *A&A*, 547, A51
- Groves, B., Dopita, M. A., Sutherland, R. S., Kewley, L. J., Fischera, J., Leitherer, C., Brandl, B., & van Breugel, W. 2008, *ApJS*, 176, 438
- Haardt, F., & Madau, P. 1996, *ApJ*, 461, 20
- Heckman, T. M. 2001, in *Astronomical Society of the Pacific Conference Series*, Vol. 240, *Gas and Galaxy Evolution*, ed. J. E. Hibbard, M. Rupen, & J. H. van Gorkom, 345
- Hinshaw, G., Larson, D., Komatsu, E., Spergel, D. N., Bennett, C. L., Dunkley, J., Nolta, M. R., Halpern, M., Hill, R. S., Odegard, N., Page, L., Smith, K. M., Weiland, J. L., Gold, B., Jarosik, N., Kogut, A., Limon, M., Meyer, S. S., Tucker, G. S., Wollack, E., & Wright, E. L. 2012, *ArXiv e-prints*
- Hodge, J. A., Karim, A., Smail, I., Swinbank, A. M., Walter, F., Biggs, A. D., Ivison, R. J., Weiss, A., Alexander, D. M., Bertoldi, F., Brandt, W. N., Chapman, S. C., Coppin, K. E. K., Cox, P., Danielson, A. L. R., Dannerbauer, H., De Breuck, C., Decarli, R., Edge, A. C., Greve, T. R., Knudsen, K. K., Menten, K. M., Rix, H.-W., Schinnerer, E., Simpson, J. M., Wardlow, J. L., & van der Werf, P. 2013, *ApJ*, 768, 91
- Jonsson, P. 2006, *MNRAS*, 372, 2
- Jonsson, P., Groves, B. A., & Cox, T. J. 2010, *MNRAS*, 403, 17
- Joung, M. R., Cen, R., & Bryan, G. L. 2009, *ApJ*, 692, L1
- Kimm, T., & Cen, R. 2013, *ArXiv e-prints*

- Komatsu, E., Smith, K. M., Dunkley, J., Bennett, C. L., Gold, B., Hinshaw, G., Jarosik, N., Larson, D., Nolta, M. R., Page, L., Spergel, D. N., Halpern, M., Hill, R. S., Kogut, A., Limon, M., Meyer, S. S., Odegard, N., Tucker, G. S., Weiland, J. L., Wollack, E., & Wright, E. L. 2010, ArXiv e-prints
- Krauss, L. M., & Turner, M. S. 1995, *General Relativity and Gravitation*, 27, 1137
- Labbé, I., González, V., Bouwens, R. J., Illingworth, G. D., Franx, M., Trenti, M., Oesch, P. A., van Dokkum, P. G., Stiavelli, M., Carollo, C. M., Kriek, M., & Magee, D. 2010, *ApJ*, 716, L103
- Leitherer, C., Schaerer, D., Goldader, J. D., Delgado, R. M. G., Robert, C., Kune, D. F., de Mello, D. F., Devost, D., & Heckman, T. M. 1999, *ApJS*, 123, 3
- McLure, R. J., Dunlop, J. S., de Ravel, L., Cirasuolo, M., Ellis, R. S., Schenker, M., Robertson, B. E., Koekemoer, A. M., Stark, D. P., & Bowler, R. A. A. 2011, *MNRAS*, 418, 2074
- Ono, Y., Ouchi, M., Curtis-Lake, E., Schenker, M. A., Ellis, R. S., McLure, R. J., Dunlop, J. S., Robertson, B. E., Koekemoer, A. M., Bowler, R. A. A., Rogers, A. B., Schneider, E., Charlot, S., Stark, D. P., Shimasaku, K., Furlanetto, S. R., & Cirasuolo, M. 2012, ArXiv e-prints
- O’Shea, B. W., Abel, T., Whalen, D., & Norman, M. L. 2005, *ApJ*, 628, L5
- Planck Collaboration, Ade, P. A. R., Aghanim, N., Armitage-Caplan, C., Arnaud, M., Ashdown, M., Atrio-Barandela, F., Aumont, J., Baccigalupi, C., Banday, A. J., & et al. 2013, ArXiv e-prints
- Razoumov, A. O., & Sommer-Larsen, J. 2010, *ApJ*, 710, 1239
- Stark, D. P., Ellis, R. S., Chiu, K., Ouchi, M., & Bunker, A. 2010, *MNRAS*, 408, 1628
- Trujillo, I., Förster Schreiber, N. M., Rudnick, G., Barden, M., Franx, M., Rix, H., Caldwell, J. A. R., McIntosh, D. H., Toft, S., Häußler, B., Zirm, A., van Dokkum, P. G., Labbé, I., Moorwood, A., Röttgering, H., van der Wel, A., van der Werf, P., & van Starckenburg, L. 2006, *ApJ*, 650, 18
- Turk, M. J., Smith, B. D., Oishi, J. S., Skory, S., Skillman, S. W., Abel, T., & Norman, M. L. 2011, *ApJS*, 192, 9
- Weingartner, J. C., & Draine, B. T. 2001, *ApJ*, 548, 296
- Wilkins, S. M., Bunker, A. J., Stanway, E., Lorenzoni, S., & Caruana, J. 2011, *MNRAS*, 417, 717
- Wise, J. H., & Cen, R. 2009, *ApJ*, 693, 984
- Yajima, H., Choi, J.-H., & Nagamine, K. 2011, *MNRAS*, 412, 411
- Yan, H., Yan, L., Zamojski, M. A., Windhorst, R. A., McCarthy, P. J., Fan, X., Röttgering, H. J. A., Koekemoer, A. M., Robertson, B. E., Davé, R., & Cai, Z. 2010, ArXiv e-prints

